applied sciences

MDPI

Article

Design and Optimization of a Dual-Input Coupling Powertrain System: A Case Study for Electric Tractors

Tonghui Li, Bin Xie *, Zhen Li and Jiakun Li

College of Engineering, China Agricultural University, Beijing 100083, China; 18630225356@163.com (T.L.); zhenli@cau.edu.cn (Z.L.); ljk17864305216@163.com (J.L.)

* Correspondence: xiebincau@126.com

Received: 28 January 2020; Accepted: 25 February 2020; Published: 28 February 2020

Abstract: In this study, a dual-input coupling powertrain system (DICPS) was proposed to improve the energy utilization efficiency of pure electric tractors (PETs). The working principles of the DICPS under different modes were analyzed and dynamic models were established. To study the influence of changing key parameters in the DICPS on the economic performance of PETs, a parameter-matching design method was proposed and the feasible region of the design parameters was determined according to the tractor's dynamic performance. In addition, we put forward an energy management strategy (EMS) based on the optimal system efficiency and a dual-motor-driven electric tractor (DMET) model was built in MATLAB/Simulink. The simulation results revealed that different parameter configurations of DICPS will lead to significant changes in overall efficiency, with a maximum difference of 6.6% (under a rotary tillage cycle). We found that the optimal parameter configuration for the DMET under two typical working conditions was PDR = 0.5, k = 1.6. Compared with the single-motor powertrain system (SMPS), the DICPS with the optimal configuration of key parameters can significantly improve overall efficiency by about 9.8% (under a plowing cycle).

Keywords: electric tractor; dual-input coupling powertrain; parameter optimization; quadratic programming algorithm

1. Introduction

In recent years, the number of tractors of different forms has greatly increased, as they are the main type of agricultural power machinery. The inefficiency and high fuel consumption of traditional tractors lead to energy waste and environmental pollution [1]. A tractor uses 345,000 kL of oil, accounting for 48.5% of the total oil consumption of agricultural machines. Thus, developing an efficient tractor is necessary [2].

Battery-powered electric vehicles have been proven to be one of the most effective ways to reduce emissions and energy consumption. With the rapid development of battery technology and motor technology, there is growing interest in the electrification of agricultural tractors [3]. Pure electric tractors (PETs) seem to be a promising solution in the context of more sustainable farming as they can use a wide range of power sources which can be obtained from a variety of renewable or clean energy sources [4]. However, at the current technical level, the biggest bottleneck in the development of PET is their limited operation time. Optimizing transmission efficiency is a practical method to increase operation time before the energy density of the battery displays evident improvement. The improvement of transmission efficiency depends on the development of an efficient powertrain and effective control strategies.

At present, the powertrains of PETs on the market are mostly driven by a single motor, whereby the diesel engine is replaced by batteries and a motor and the original multi-gear transmission is retained [5–7]. Considering the different power requirements of tractors under various working

conditions, the motor often works in a low-efficiency region under low-load conditions. Moreover, research shows that the tractors' multi-speed mechanical gearboxes will bring more energy losses [8]. It has been found that in the powertrain configuration of "single motor + multi-speed transmission", it is difficult to change the current situation of tractors, whereby they present low efficiency and high power consumption. Therefore, it is necessary to find other powertrain structures that can improve tractor efficiency. Many studies have shown that dual-input coupling powertrain systems (DICPSs) have been widely used in electric vehicles to reduce energy consumption and improve efficiency [9–12]. By using two smaller motors instead of a single high-power source, the torque capacity of a single motor can be reduced, which is beneficial to the development of high-speed motors, thereby increasing the power density of the driving system. Moreover, the operating points of the two motors can be adjusted to optimize the efficiency of the drive system.

Most studies on DICPS in the agricultural tractor field have focused on hybrid tractors, while the PET concept is applied less frequently. Lee et al. designed a powertrain simulation model and proved the fuel consumption reduction of the parallel hybrid tractor through the power distribution ratio strategy. The results showed that the fuel efficiency of the hybrid tractor was 11.78% higher than the conventional tractor [13]. Lee et al. developed a parallel hybrid tractor, which had three control modes: idle, power assist, and battery charge. The results showed that the performance of the hybrid tractor was better than the conventional tractor at the higher load condition, and the fuel efficiency was 74% lower than that of the conventional tractor [2]. Deng et al. designed a parallel hybrid tractor transmission system with a planetary gear set as the power coupling device, and a design theory and calculation method for the transmission system were proposed. The simulation results showed that the hybrid tractor could save energy by up to 24% under plowing operations compared to the equivalent power fuel tractor [14].

The literature studies described above show that hybrid tractors with a dual-input powertrain can effectively improve fuel efficiency. However, hybrid tractors do not meet the development trend of new energy vehicles for zero emissions. Moreover, the motors of hybrid tractors are mainly used as an auxiliary power source to improve the fuel efficiency of the engine, which cannot fully provide the characteristics of high efficiency and motor precision. Therefore, the DICPS was adopted to improve the overall efficiency of PETs. When the power demand is low, the PET can be driven by a single motor to increase the torque utilization factor of the motor. When the power demand is high, the PET can be driven by two motors to improve the operating efficiency of the DICPS.

After the powertrain structure is determined, reasonable parameter sizing and control strategies are necessary to realize efficient operation of the dual-motor-driven electric tractor (DMET). However, the parameter-matching design method of a conventional tractor was not entirely suitable for DMET. For conventional tractors, only the dynamic performance indexes need to be satisfied, but the parameter matching of DICPSs should not only consider the dynamic indexes, but also the high-efficiency region distribution of the two motors [15,16]. Chen et al. proposed a method of powertrain parameter-matching and optimization design for a dual-motor-driven electric tractor, and used a particle swarm optimization algorithm based on a mixed penalty function to optimize the parameters [17]. The results showed that the selected optimization objectives had made evident progress after the optimization. However, they did not optimize the structure parameters according to the actual working condition data of the tractor. Therefore, it is necessary to study the matching optimization between the high-efficiency region of the two motors and the actual working conditions of the tractor.

There have been some studies on control strategies for DICPSs. Wu et al. proposed a real-time control strategy for a dual-input power-split transmission system [18]. The control strategy improved the overall efficiency of the vehicle at low speed and at frequent deceleration. However, the three PI controllers required a lot of debugging to obtain the best control parameters, a time-consuming process that was not able to guarantee robustness and timeliness. Zhang et al. used Pontryagin's minimum principle (PMP) algorithm to optimize the control strategy of an electric bus driven by two motors under three driving cycles [19]. Jia et al. proposed optimization-based energy management strategies

for hybrid electric agricultural tractors to minimize fuel consumption in typical working cycles [20]. Compared with the typical rule-based strategy, these optimal energy management strategies (EMSs) showed significant improvements in fuel efficiency. Both PMP and Dynamic programming (DP) strategies require information of the entire cycle condition, and can only achieve global optimization under specific conditions. Computational complexity makes real-time operation difficult to achieve.

The objectives of this study were to design a DICPS for a PET which could improve the PET's economic performance without compromising its dynamic performance. Furthermore, the system needs a reasonable parameter configuration and an effective energy management strategy to ensure the efficient operation of the PET. Furthermore, this study aimed to find the optimal parameter configuration for tractor working conditions through simulation experiments.

The paper is organized as follows: Section 2.1 introduces the overall configuration of the DICPS. The modeling and driving modes of the DICPS are displayed in Section 2.2. The system parameters are matched and determined in Section 2.3. In Section 2.4, an EMS developed to minimize power loss and maximize overall system efficiency is explained. The simulation results and discussion are given in Section 3, where two typical working conditions were used to validate the effectiveness of the proposed method. Finally, conclusions are presented in Section 4.

2. Materials and Methods

2.1. Configuration of the DICPS

The overall configuration of the DICPS is shown in Figure 1; it was mainly composed of two motors, EM_S and EM_R; two brakes, B1 and B2; and the dynamic coupling gearbox. EM_S and EM_R were powered by a Li-ion battery pack and connected with the sun gear and ring gear, respectively, through reduction gears, and the carrier was the output of the powertrain. The power take-off (PTO) was connected to EM_S or EM_R through the reduction gear to provide output power for tractor farming operations. Due to the wide speed range and fast torque response of the motors, the multi-gear transmission found in a conventional tractor was removed, saving space and reducing weight and costs.

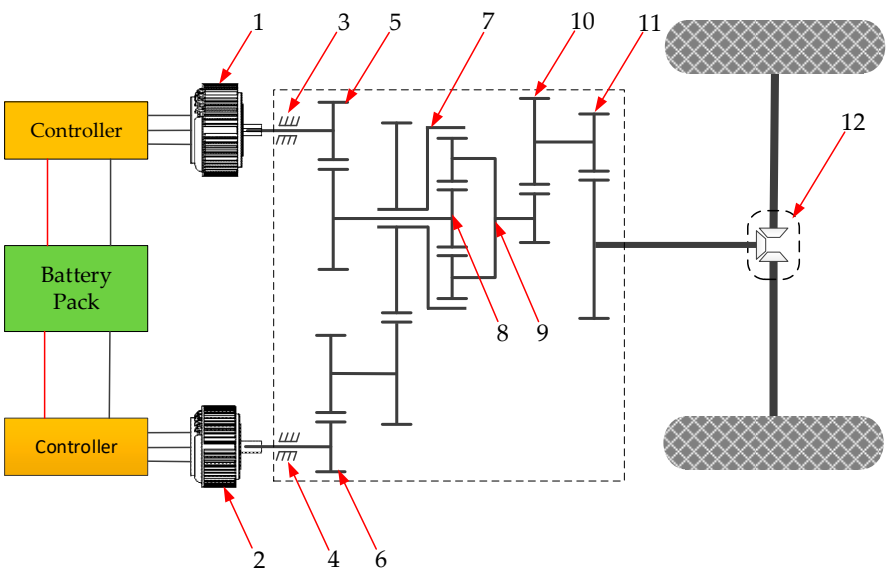

Figure 1. Schematic diagram of DICPS. 1. EM_S; 2. EM_R; 3. B1; 4. B2; 5. Reduction gear for EM_S i_s; 6. Reduction gear for EM_R i_r; 7. Ring gear; 8. Sun gear; 9. Carrier; 10. Main reduction gear i_m; 11. Final reduction gear i_f; 12. Differential mechanism.

2.2. Modeling and Modes Analysis

2.2.1. Tractor Dynamic Model

As agricultural vehicles, tractors experiences different resistances to automobiles—mainly including traction resistance, rolling resistance, and slope resistance—which can be expressed by Equation (1). It is noteworthy that tractors travel slowly, so air resistance is neglected.

$$\begin{cases} m\dot{v}_a = \frac{T_c i_m i_f \eta_t - T_L}{r_q} \\ T_L = (F_T \cos\beta + mg\sin\theta + f(mg + F_T \sin\beta))r_q \end{cases} \tag{1}$$

where T_c denotes the output torque of the carrier, T_L is the driving resistance torque, η_t is transmission efficiency, m denotes the tractor mass, v_a is the actual velocity, r_q represents the radius of the driving wheel, F_T is the traction resistance, β refers to the angle between traction resistance and the horizontal direction, θ is the incline angle of the road, g is the gravity acceleration, and f is the rolling friction coefficient.

2.2.2. Dynamic Model of Planetary Gear Set

The static kinematics model of the planetary gear set, determined by the lever analysis method [21], can be expressed as

$$\begin{cases} k\omega_r + \omega_s = (k+1)\omega_c \\ \frac{T_c}{k+1} = \frac{T_r}{k} = T_s \\ k\omega_r - \omega_s = (k-1)\omega_p \end{cases} \tag{2}$$

where k denotes the characteristic parameter of planetary gear set; the subscripts r, s, c and p represent the ring gear, sun gear, carrier and pinion, respectively; and ω and T refer to the rotation speed and torque, respectively.

Since the static model does not take into account the dynamic response of components, there will be a large deviation when the acceleration of gears is very large, and the two inputs of the planetary gear set are controlled by two motors independently, so Equation (2) cannot meet the actual dynamic response. When the speed and acceleration are given, the working points of EM_S and EM_R are not uniquely determined. In order to make EM_S and EM_R work in the optimum conditions to minimize power consumption, a dynamic model of the planetary gear was essential. The dynamic model can be expressed as

$$\begin{cases} I_r\dot{\omega}_r = T_r - T_{cr} \\ I_s\dot{\omega}_s = T_s - T_{cs} \\ I_p\dot{\omega}_p = \frac{k-1}{2k}T_{cr} - \frac{k-1}{2}T_{cs} \\ \left(I_c + I_{ps}\right)\dot{\omega}_c = \frac{k+1}{2}T_{cs} + \frac{k+1}{2k}T_{cr} - T_c \end{cases} \tag{3}$$

where I_r, I_s, and I_c are the equivalent inertia on the ring gear, sun gear, and carrier, respectively; I_p denotes the inertia of the pinion relative to the center of mass; I_{ps} is its inertia relative to the center of sun gear; and T_{cr} and T_{cs} are the inner torques.

2.2.3. Battery Model

The thermal temperature effect and battery life were ignored in this paper, and the basic physical model of battery was simplified as a voltage source with open circuit voltage and internal resistance, both of which depend on the battery SOC, so the mathematical model of the battery can be expressed as

$$\dot{SOC} = -\frac{U_{oc} - \sqrt{{U_{oc}}^2 - 4R_{bat} \cdot P_{bat}}}{2R_{bat} \cdot Q_{bat}} \tag{4}$$

where U_{oc} is the battery open circuit voltage; R_{bat} is the internal resistance; P_{bat} is the output power of the battery, which is also the electric power consumed by the two motors; Q_{bat} is the capacity of battery; and the index t represents any time instant.

It is worth noting that both U_{oc} and R_{bat} can be obtained from the look-up table of the battery SOC, and the instantaneous internal energy of battery P_e can then be obtained as

$$P_e = -U_{oc}Q_{bat}\dot{SOC} \tag{5}$$

2.2.4. Efficiency Model

Since this paper mainly focused on the influence of the selection of a dual-motor coupling powertrain on the economic performance of a PET, it was necessary to establish efficiency models of a DICPS, including a motor efficiency model and a transmission efficiency model.

To obtain the efficiency model of the motor, we measured the output torque, speed, bus voltage, and current of the motor through a bench test and calculated the efficiency value. The motor efficiency was defined as the function of output speed and torque, as shown in Equation (6), and the efficiency in a certain state was obtained by the interpolation method. The efficiency map of motors in this study is shown in Section 2.3.1.

$$\eta_m = f(\omega_m, T_m) \tag{6}$$

where T_m and ω_m denote the output torque and output rotation speed of the motor, respectively.

Here, we only considered the gear efficiency in the coupling box, including the dynamic efficiency of the planetary gear set and the efficiency of the reduction gears. For a pair of gears, one of the most widely used efficiency models is as follows [22].

$$\eta = 1 - \left|\frac{1}{5}\left(\frac{1}{z_a} \pm \frac{1}{z_b}\right)\right| \tag{7}$$

where Z_a and Z_b represent the number of teeth, and the ± symbol indicates external (+) and internal gear pairs (−). In terms of the planetary gear set, there are different control strategies and energy losses for different design parameters and driving modes, so an efficiency model should be established for each of the three driving modes.

$$\begin{cases} \eta_{r(s-c)} = 1 - \frac{k\cdot(1-\eta_{c(s-r)})}{1+k} & M1S \\ \eta_{s,r-c} = 1 - \left|\frac{\frac{\omega_{m1}}{i_s} - \omega_c}{\frac{\omega_{m1}}{i_s} + k\frac{\omega_{m2}}{i_r}}\right|(1-\eta_{c(s-r)}) & DMC \\ \eta_{s(r-c)} = 1 - \frac{1-\eta_{c(s-r)}}{1+k} & M2S \end{cases} \tag{8}$$

where $\eta_{r(s-c)}$ indicates the efficiency when the ring gear is fixed, power is input into the sun gear, and output from the planet carrier; $\eta_{c(s-r)}$ is the efficiency when the planet carrier is fixed with power inputs into the sun gear and outputs from the ring gear; $\eta_{s(r-c)}$ denotes the efficiency when the sun gear is fixed and power is input into the ring gear and output from the planet carrier; and $\eta_{s,r-c}$ denotes the efficiency when power is input into the ring gear and sun gear and output from the planet carrier.

2.2.5. Driving Mode Analysis

The advantage of placing the brakes B1 and B2 on the output shafts of EM_S and EM_R rather than directly on the ring and sun gears is that the required braking torque is reduced proportionally through the reduction gears, so smaller brakes can be used. By controlling brakes B1 and B2, the DICPS can operate in three driving modes: EM_S independent drive (M1S), EM_R independent drive (M2S), and dual-motor coupling drive (DMC). Table 1 shows the working status of each component in each driving mode.

Table 1. System operation status.

Working Mode	EM_S	EM_R	B1	B2
M1S	•	o	o	•
M2S	o	•	•	o
DMC	•	•	o	o

• indicates that the motor is on or the brake is engaged; o indicates that the motor is off or the brake is disengaged.

When the DICPS works in mode M1S, brake B1 is disengaged, B2 is engaged, EM_S is on, and EM_R is off. The DICPS can amplify the output torque of EM_S through the planetary mechanism to provide a high torque output, which is suitable for low-speed and high-torque operation conditions such as plowing. The power flow is shown in Figure 2a, and the dynamic model of DICPS in M1S mode was obtained based on the dynamic model of the planetary gear set.

$$\begin{cases} (T_{m1} - I_{m1}\dot{\omega}_{m1}) \cdot i_s(1+k) - \frac{T_L}{i_f i_m} = I_c\dot{\omega}_c \\ I_c\dot{\omega}_c = \frac{m{r_q}^2}{{i_f}^2{i_m}^2} \cdot \frac{\dot{v}_a i_f i_m}{r_q} = \frac{m r_q \dot{v}_a}{i_f i_m} \\ \omega_{m1} = \frac{v_a i_f i_m}{r_q} \cdot i_s(1+k) \end{cases} \tag{9}$$

where T_{m1} and ω_{m1} are the output torque and the speed of EM_S, respectively, and I_{m1} is the equivalent inertia of EM_S.

When the DICPS operates in mode M2S, EM_S closes and EM_R operates, B1 engages to brake the ring gear, and B2 is disengaged. Figure 2b shows the power flow. The dynamic model of DICPS in M2S mode is as follows.

$$\begin{cases} (T_{m2} - I_{m2}\dot{\omega}_{m2}) \cdot i_r \frac{1+k}{k} - \frac{T_L}{i_f i_m} = \frac{m r_q \dot{v}_a}{i_f i_m} \\ \omega_{m2} = \frac{v_a i_f i_m i_r}{r_q} \cdot \frac{1+k}{k} \end{cases} \tag{10}$$

where I_{m2} is the equivalent inertia of EM_R, T_{m1} and ω_{m1} are the output torque and the speed of EM_R.

When the DICPS works in DMC mode, two motors operate simultaneously and the brakes B1 and B2 are disengaged. At this time, the output power of EM_S and EM_R is combined by the planetary gears. This mode can achieve a higher speed under medium and low loads, which is suitable for transshipment and transportation operations. Figure 2c shows the power flow. The dynamic model of the DICPS in DMC mode can be expressed as

$$\begin{cases} (\min(T_{m1} i_s, T_{m2} i_r/k) - I_{m1}\dot{\omega}_{m1} i_s - I_{m2}\dot{\omega}_{m2} i_r/k)(1+k) = \frac{m r_q \dot{v}_a + T_L}{i_f i_m} \\ \omega_{m1}/i_s + k\omega_{m2}/i_r = (1+k)\frac{v_a i_f i_m}{r_q} \end{cases} \tag{11}$$

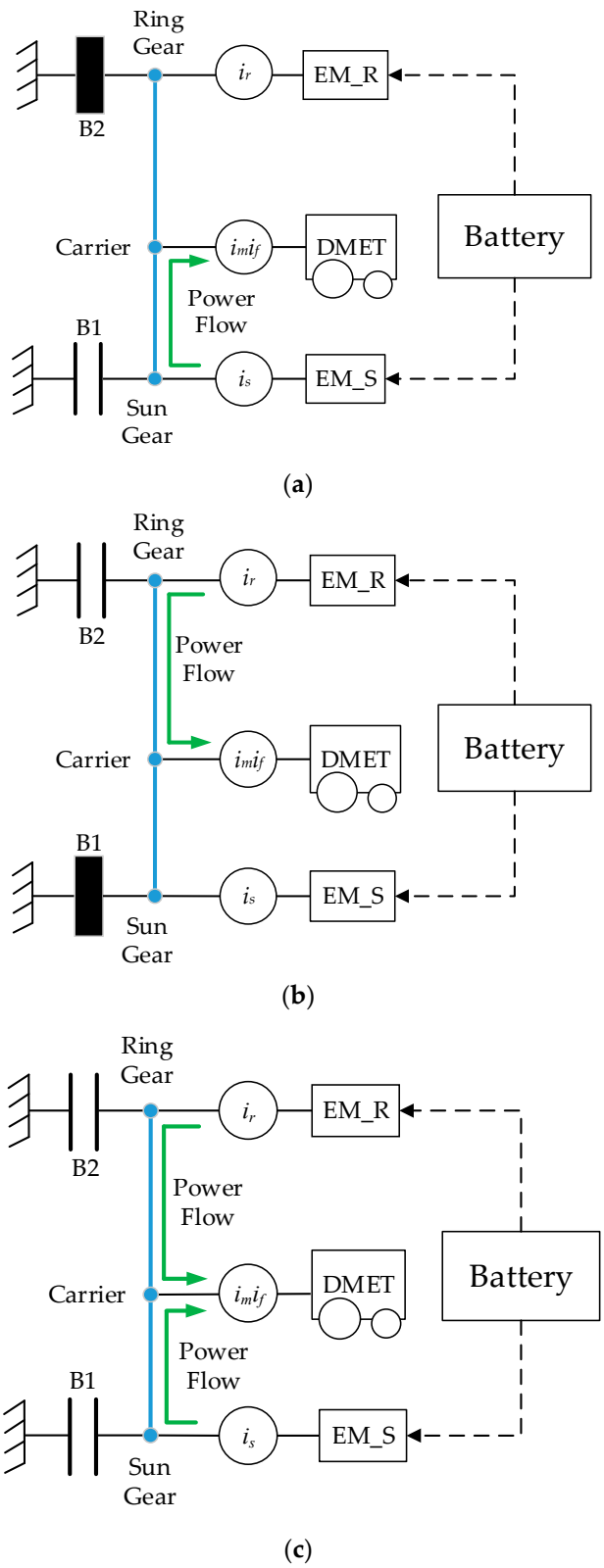

Figure 2. (**a**) Power flow in M1S mode. (**b**) Power flow in M2S mode. (**c**) Power flow in DMC mode.

2.3. Parameter Matching of DICPS

Unlike cars or engineering vehicles, tractors are mainly used for farmland operations and road transportation; the resistance loads are different under different operating conditions [23].

The performance of the DICPS is closely related to the parameter design of components such as the motors and the power-coupled gearbox. Correct selection of these parameters can effectively improve the dynamic and economic performance of the DMET.

2.3.1. Motor Parameter Matching

A 40 hp tractor was the subject of this study, and its rated power was 29.8 kW. In order to evaluate the economic performance of the DICPS, a single-motor two-speed powertrain system (SMPS) was proposed as the benchmark, which mainly included a motor EM_T and a two-speed mechanical transmission; its main parameters are listed in Table 2. The maximum draft force at 10 km/h was determined to be 12,731.3 N through numerical calculation, and the maximum speed was about 31.25 km/h, which can meet the dynamic performance indexes of tractors.

Table 2. Powertrain specifications of SMPS.

Components	Parameters	Value
Motor	Rated/peak power (kW)	30/49
	Rated/maximum torque (Nm)	100/200
	Rated/maximum speed (rpm)	2300/7500
Transmission	1 gear ratio	3.3
	2 gear ratio	2.294
	Main reduction gear i_m	2.67
	Final reduction gear i_f	5.0714

To make a fair comparison between the proposed DICPS and SMPS, the summed power of EM_S and EM_R was equal to the power of EM_T. However, the power ratio between the two motors in the summed power, defined as PDR using Equation (12), was uncertain. To study the effect of different power ratios on the dynamic and economic performance of the DICPS, we set five PDRs here: 0.2, 035, 0.5, 0.65, and 0.8.

$$PDR = \frac{P_{\max 1}}{P_{\max 1} + P_{\max 2}} \tag{12}$$

where $P_{\max 1}$ and $P_{\max 2}$ denote the maximum power of EM_S and EM_R, respectively.

To simplify the model, the efficiency MAPs of EM_S and EM_R were defined as having the same shape as EM_T. The speed range of the two motors was the same as that of EM_T, but the torques were proportional to EM_T, i.e., $T_{\max 1} = PDR \cdot T_{\max,t}$, $T_{\max 2} = (1\text{-}PDR) \cdot T_{\max,t}$. The efficiency map of EM_T is shown in Figure 3.

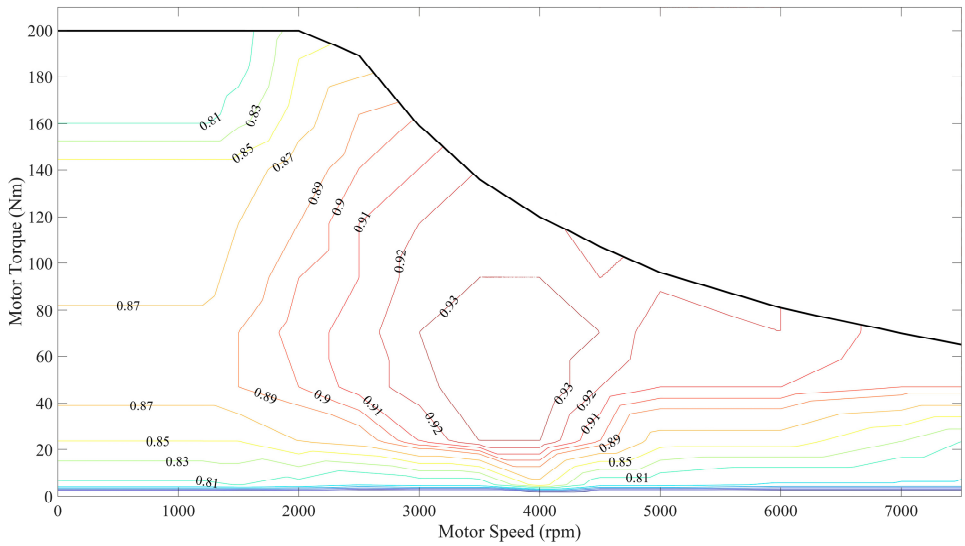

Figure 3. Efficiency map of EM_T in SMPS.

2.3.2. Gear Ratio Matching

Since tractors often work in heavy-duty working conditions, such as plowing, requiring a large amount of power over a long duration, gear ratios should be reasonably designed to satisfy the demand power of DMETs within sufficient speed ranges. As can be seen from Equations (7)–(9), the dynamic performance of the DICPS mainly depends on k, i_r, i_s, i_m, and i_f, where i_m and i_f are the same as those in SMPS. Since the values of i_r and i_s are closely related to the size of k, and to verify the effect of k on the economy of DICPS, we set the feasible range of k as (1.6, 7.6).

The maximum output torque of the DICPS in the three driving modes was

$$\begin{cases} T_{c\max,s} = (1+k)i_s T_{\max1}(\omega_{m1}) & M1S \\ T_{c\max,r} = (1+k)i_r T_{\max2}(\omega_{m2})/k & M2S \\ T_{c\max,D} = \min(T_{c\max,s}, T_{c\max,r}) & DMC \end{cases} \tag{13}$$

where $T_{c\max,s}$, $T_{c\max,r}$, and $T_{c\max,D}$ denote the maximum output torque in the M1S mode, the M2S mode, and the DMC mode, respectively, and $T_{\max1}$ and $T_{\max2}$ denote the maximum output torque of EM_S and EM_R.

In the DMC mode, both motors are active at the same time. Although their speed can be independently controlled, their torque depends entirely on the required output torque, as shown in Equation (2). As a result, the branch with the smallest torque capacity limits the maximum torque output of this mode. In order to maximize the operating range of the dual-motor driving mode, the gear ratio i_r and i_s must be reasonably selected so that $T_{c\max,s} = T_{c\max,r}$.

$$\frac{i_s}{i_r} = \frac{1}{k} \cdot \frac{T_{\max2}}{T_{\max1}} \tag{14}$$

As can be seen from Figure 3, the available torque of the motor varies with speed and the motor can provide a constant maximum torque from the stationary point to the rated speed. The available torque then decreases with the increase of the motor speed. Since tractors have the characteristics of low speed and high torque in field operations, the speed range is mainly 0.8–10 km/h. Therefore, to provide the maximum available torque for the DICPS in heavy-duty operations, both motors should run at less than the rated speed. The restriction can be expressed as

$$\frac{\omega_{e1}}{i_s} + \frac{\omega_{e2}}{i_r}k \geq \frac{10}{3.6 \cdot r_q} \cdot i_m i_f (1+k) \tag{15}$$

where ω_{e1} and ω_{e2} are the rated speed of EM_S and EM_R, respectively.

To ensure that the DICPS can provide sufficient power for plowing and other heavy-duty operations, the maximum torque limit for plowing, at the maximum operating speed of 10 km/h, can be expressed as

$$\begin{cases} i_m i_f T_{c\max}(v) \geq F_{total} \cdot r_q \\ F_{total} = F_{T\max} + mgf \\ F_{T\max} = 1.2 \cdot (Zb_1 h_s s_r) \end{cases} \tag{16}$$

where F_{total} is the total resistance on the tractor, F_{Tmax} refers to the maximum tractive force, Z is the number of plowshares, b_1 is the ploughshare width, h_s is the tillage depth, and s_r is the soil-specific resistance.

To ensure that the DMET can reach a maximum speed of 30 km/h, the relationship between the maximum output speed of the DICPS and gear ratios needs to be satisfied as follows.

$$\begin{cases} \frac{(\omega_{\max 1}/i_s + k\omega_{\max 2}/i_r)}{1+k} = \omega_{\max,c} \\ \omega_{\max,c} \geq \frac{V_{\max} i_f i_m}{3.6 r_w} \end{cases} \tag{17}$$

where $\omega_{\max 1}$, $\omega_{\max 2}$, and $\omega_{max,c}$ represent the maximum rotational speed for EM_S, EM_R, and the carrier, respectively, and V_{max} is the maximum speed of the tractor.

Tractors need to meet the maximum gradient requirements in road transport conditions. The required gear ratios to propel a DMET on a 15% grade road at 10 km/h can be expressed as

$$\begin{cases} i_m i_f T_{c\max}(v) \geq F_{total} \cdot r_q \\ F_{total} = (G_n + G_s)(f\cos\theta + \sin\theta) \\ v = 10/3.6, \theta = 15 \end{cases} \tag{18}$$

where G_n is the total weight of the trailer and G_s is the weight of the tractor.

On the basis of different PDR and K values, the feasible region of i_s and i_r satisfying Equations (13)–(18) was obtained, as shown in Table 3. In this case, the DMET can produce a maximum traction force of 14,319 N and a maximum speed of 30.6 km/h, which can satisfy the power requirements of a 40 hp tractor.

Table 3. Gear ratios of i_s and i_r.

		PDR = 0.2	PDR = 0.35	PDR = 0.5	PDR = 0.65	PDR = 0.8
i_s	k = 1.6	5.49	3.14	2.198	1.69	1.37
	k = 3.6	3.1	1.77	1.24	0.96	0.78
	k = 5.6	2.16	1.237	0.866	0.666	0.541
	k = 7.6	1.661	0.949	0.665	0.511	0.415
i_r	k = 1.6	2.198	2.70	3.516	5.023	8.791
	k = 3.6	2.795	3.44	4.472	6.388	11.18
	k = 5.6	3.03	3.729	4.848	6.926	12.121
	k = 7.6	3.156	3.885	5.049	7.214	12.625

2.4. Energy Management Strategy

Energy-efficient operation of a DICPS depends on two crucial elements: a good choice of operating mode (dual-motor or single-motor operation) and, in dual-motor operation, a well-selected power distribution. Therefore, a real-time energy management strategy was introduced to improve the overall efficiency of the DMET, which consisted of power distribution control and mode stability control.

2.4.1. Power Distribution Control

When the DICPS works in single-motor driving mode (M1S, M2S), the output power of the motor is directly determined by the required speed and torque of the driving wheels, without power distribution. When the DICPS is in dual-motor coupling driving mode, the output power of both motors can be valued within a certain range. It is necessary to determine the power flow between two motors. As a pure electric tractor, the output power of the battery, composed of consumed power and charging power, can be expressed as

$$P_{bat} = \left(T_{m1}\omega_{m1}\eta_{m1}{}^{-sign(\omega_{m1}T_{m1})} + T_{m2}\omega_{m2}\eta_{m2}{}^{-sign(\omega_{m2}T_{m2})}\right)/9550 \tag{19}$$

According to Equations (4), (5), and (19), the internal power consumption of the battery can be obtained, and the optimal control problem can be formulated as

$$\begin{cases} \min\limits_{u}(J_c = \int_{t_0}^{t_f} c(x(t), u(t))dt) \\ c(x(t), u(t)) = P_e \end{cases} \tag{20}$$

The goal was to find the control set u that would minimize the cost J_c, defined as the integral of a cost function over a time interval. $c(x(t), u(t))$ denotes the objective function, which is the internal energy of the battery. Four variables can be found in the objective function, i.e., T_{m1}, ω_{m1}, T_{m2}, and ω_{m2}. However, these four variables are not independent. After the tractor speed and acceleration are known, the torques of the two motors can be expressed as

$$\begin{cases} T_{m1} = \frac{I_f\dot{\omega}_f + T_L}{i_m i_f i_s(1+k)} + I_{m1}\dot{\omega}_{m1} \\ T_{m2} = \frac{k(I_f\dot{\omega}_f + T_L)}{i_m i_f i_r(1+k)} + I_{m2}\dot{\omega}_{m2} \end{cases} \tag{21}$$

where I_f denotes the equivalent inertia of tractor body including transmission components and $\dot{\omega}_f$ is the angular acceleration of the final shaft.

As to the speed, there was only one independent design variable, which was the EM_S speed in this study. Once it was determined, the EM_R speed could be calculated by

$$\begin{cases} \omega_{m2} = i_2\frac{\omega_c(1+k) - \omega_{m1}/i_1}{k} \\ \omega_c = \frac{v_a * 30}{\pi r_w} * i_m i_f \end{cases} \tag{22}$$

where v_a is the actual velocity of the tractor in m/s.

In summary, there were only two independent variables of the proposed EMS: the motor speed and the working mode. However, the selection of working mode in this study was based on the maximum overall efficiency principle, and the efficient mode was selected among the three driving modes. When both EM_S and EM_R can provide the required power of the DMET, the mode with the least power losses is automatically selected according to the optimal solution. Therefore, the speed of EM_S was chosen as the control variable, the optimization model can be rewritten as Equation (23) when the target acceleration a_t and speed v_t are decided by the working cycle.

$$\min_{\omega_{m1}} P_e(v_t, a_t, \omega_{m1}) \tag{23}$$

To ensure the safe and reasonable operation of the motors, the following inequality constraints were necessary.

$$\begin{cases} 0 \le \omega_{m1}(t) \le \omega_{\max 1} \\ 0 \le \omega_{m2}(t) \le \omega_{\max 2} \\ 0 \le \left|T_{m1}(\omega_{m1}(t))\right| \le T_{max1}(\omega_{m1}(t)) \\ 0 \le \left|T_{m2}(\omega_{m2}(t))\right| \le T_{max2}(\omega_{m2}(t)) \end{cases} \tag{24}$$

Since the design space contained many local optimal points, it was difficult to find the global optimal point using traditional optimization algorithms. Here, we used the quadratic programming algorithm to find the approximate optimal solution and calculate the instantaneous overall efficiency. The flow chart of power distribution is shown in Figure 4.

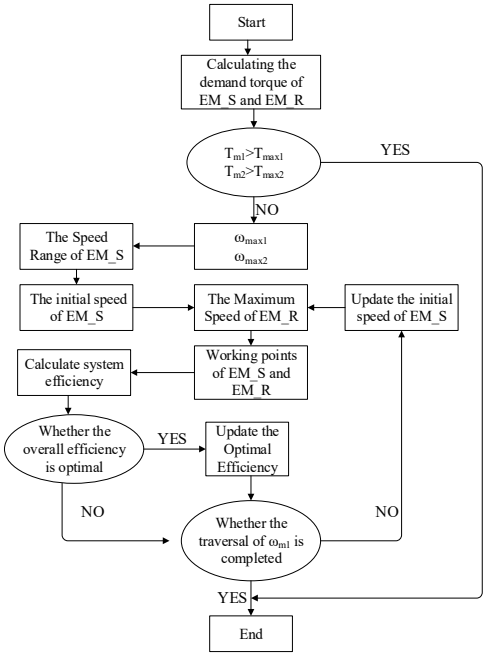

Figure 4. The flow chart of power distribution.

Figure 5 shows the curve of the objective function in the feasible area under the case that PDR = 0.65, k = 2.6, SOC = 60, and the shape of the objective function changes according to the driving conditions. According to a given speed and acceleration, the best working mode and the working points of two motors are determined by EMS. The selected working point represents the minimum power consumption. In Figure 5a, the feasible speed range of EM_S is 0–5240 rpm, and the optimal working point appears at nm1 = 0. When the acceleration is increased to 2 m/s^2, it can be seen from Figure 5b that the feasible working range of EM_S is reduced to 281 rpm to 2500 rpm. It can also be seen from the curve that Pele is significantly increased after the inflection point, for the reason that when EM_S exceeds the speed at the inflection point, EM_R will reverse to generate negative speed, and the driving system will generate cycle power, resulting in a large amount of energy waste [24,25]. When the speed is 10 km/h, the curve shows the same trend as the speed of 5 km/h as shown in Figure 5c. The optimal working point appears at nm1 = 3280 rpm; EM_S is the main power source at this point. When the acceleration increases to 2 m/s^2, the optimal working point is nm1 = 2520 rpm, and nm2 increases to 1428 rpm in the meantime.

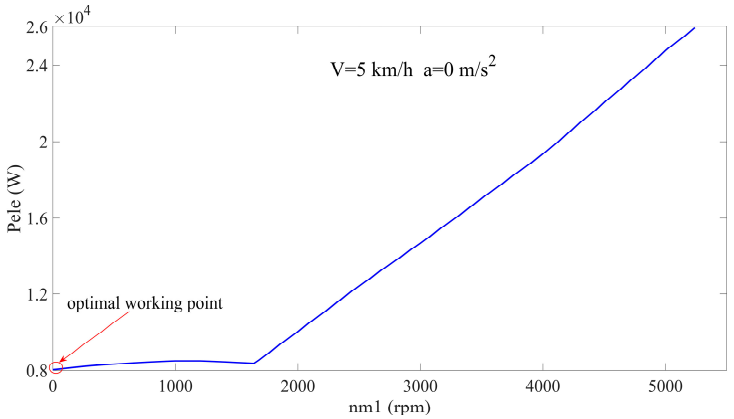

(**a**) Power consumption at V=5km/h, a=0m/s²

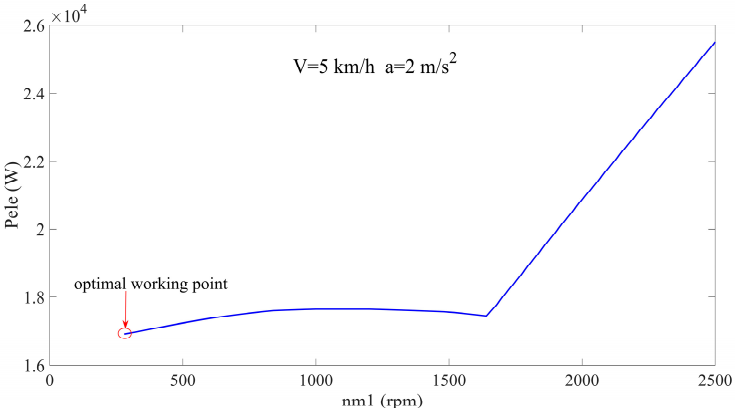

(**b**) Power consumption at V=5km/h, a=2m/s²

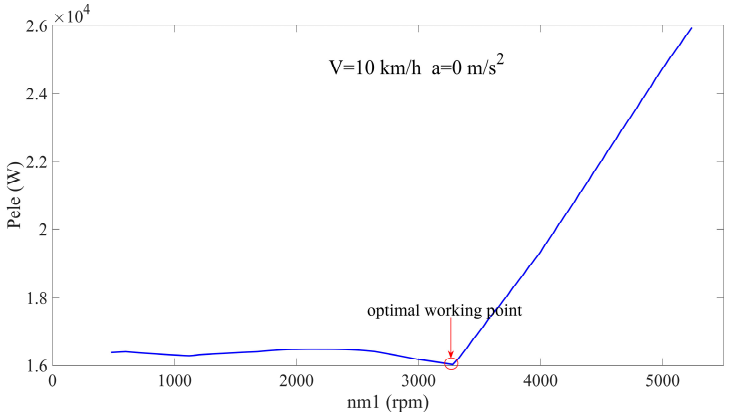

(**c**) Power consumption at V=10km/h, a=0m/s²

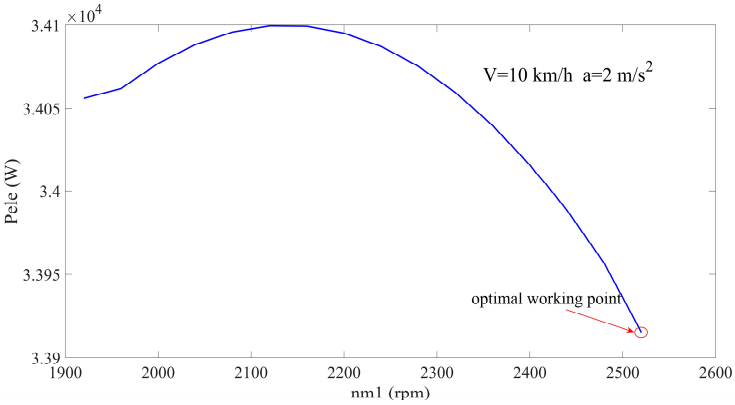

(**d**) Power consumption at V=10km/h, a=2m/s²

Figure 5. The objective function under different driving conditions (PDR = 0.65, k = 2.6, SOC = 60).

2.4.2. Mode Stability Control

The proposed real-time EMS aimed to minimize energy loss. By calculating the instantaneous power consumption of the battery in each working mode, the mode with the lowest energy consumption is selected as the current working mode. However, working conditions in the field are complex and changeable, which will cause the working mode to change frequently with the driving conditions. Excessive mode switching will cause the motor speed tooscillate greatly in a short period of time, which will affect the ride comfort of the tractor. At the same time, the operation of the electromagnetic brake will increase energy consumption, so excessive mode switching should be avoided.

The energy consumption between the current mode and the next mode is sometimes very close, and the EMS still chooses the working mode with less power consumption according to the minimum energy consumption principle, which means that the energy saved by mode switching is negligible. To solve this problem, a penalty factor was introduced into the optimization objective function to reduce unnecessary mode switching, which was only allowed in the case of obvious energy saving. To increase the mode switching threshold, the penalty factor was only applied to the non-working mode, which means that the power of the current working mode was used as the benchmark without any penalty. At the same time, the power of other modes will add extra costs, so the system may keep the current mode working when comparing the energy consumption of all the modes.

The penalty factor was defined as a step function of the power consumption variation between different operating modes, expressed as follows.

$$\lambda = \begin{cases} 0.8, & \Delta P \leq 50 \\ 1, & \Delta P > 50 \end{cases}, \qquad \Delta P = \left| P_{e_current} - P_{e_other} \right| \tag{25}$$

where λ is the penalty factor; $P_{e_current}$ and P_{e_other} denote the instantaneous energy consumption of the battery in the current working mode and non-working modes, respectively; and ΔP is the power consumption difference between the current working mode and the other two non-working modes.

The new objective function after introducing the penalty factor can be expressed as

$$P_{e_other} = \lambda^{-sign(P_e)} P_e \tag{26}$$

The simulation model for the DMET equipped with a DMCPS was implemented in MATLAB/Simulink (R2018a), as shown in Figure 6. This simulation model was mainly composed of the working cycle model, driver model, EMS model, battery model, transmission model, and the tractor dynamic model.

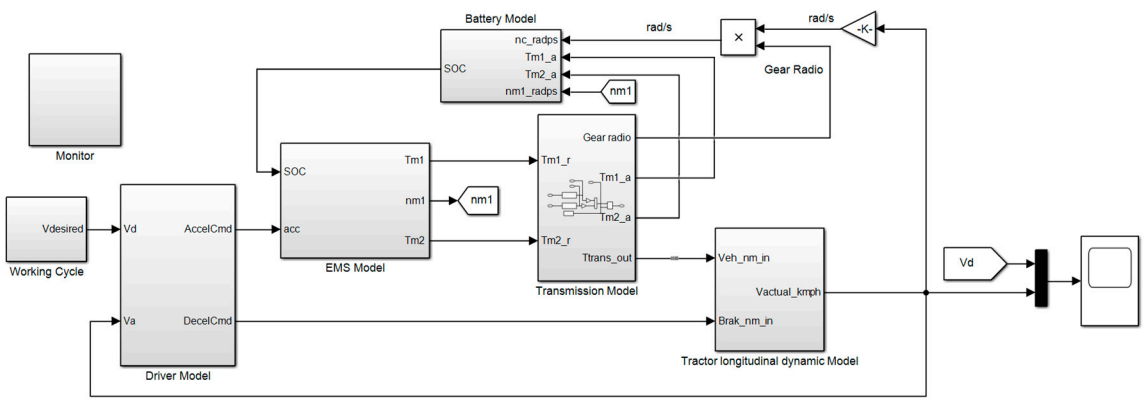

Figure 6. Simulation model for a DMET equipped with the DMCPS.

3. Results and Discussion

This section compares the economic efficiency of the DICPS under different design parameters (k, PDR) by using two typical working conditions for tractors, plowing and rotary tillage. The overall system efficiency was used as an economic evaluation indicator for the DICPS, defined as the ratio between the energy required by the DMET and the energy consumed by the motors.

$$\eta_o(t) = \frac{\int_0^t F_{total} v_a d_t}{\int_0^t P_e d_t} \tag{27}$$

where η_o is the overall efficiency of the driving system.

3.1. Plowing Cycle

Plowing is the most common and heavy-duty tractor operation. The traction resistance and tractor speed were measured in the previous field plowing to accurately simulate actual working conditions. The plowing cycle is shown in Figure 7, where the tractor operates at an average speed of 7.76 km/h under an average draft force of 2963 N. This section mainly studied the effect of different k and PDR values on the efficiency performance of DICPS in a plowing cycle.

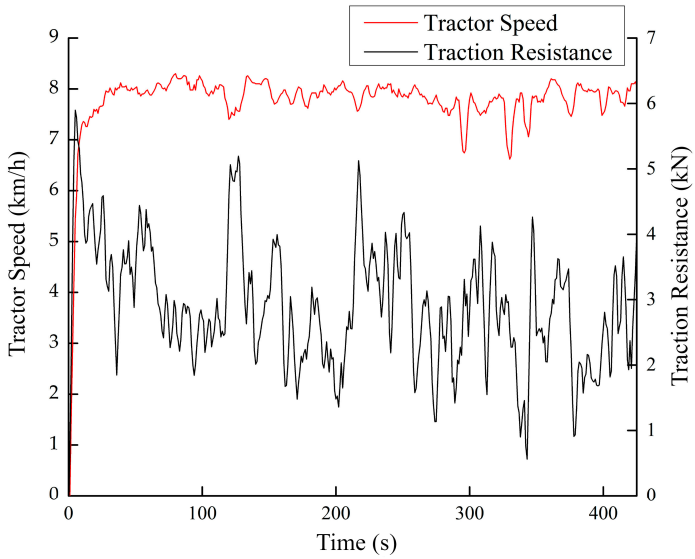

Figure 7. Plowing cycle for an agricultural tractor.

The variation in the overall efficiency with changes in k and PDR is shown in Table 4. With increasing k, the overall efficiency showed a decreasing trend. A high k further increased the output torque of EM_S and decreased the enlarging function of EM_R. This made EM_S work in high-speed and low-torque regions or make EM_R work at high-torque and low-speed regions (where the motor's efficiency is low). As a result, these high k values reduced the overall efficiency. Therefore, only the case of k = 1.6 was subsequently analyzed.

Table 4. Overview of parameter designs and their efficiency.

	PDR = 0.2	PDR = 0.35	PDR = 0.5	PDR = 0.65	PDR = 0.8
k = 1.6	85.2	87.2	87.7	87.3	85.2
k = 3.6	84.3	86	86.8	86.2	84.1
k = 5.6	83.8	85.3	86.3	85.8	83.8
k = 7.6	83.5	85	86.1	85.6	83.6

As shown in Table 4, the overall efficiency tended to increase and then decrease with increasing PDR, and the maximum value appeared at PDR = 0.5. It can be seen that the connection position of the two motors had little influence on overall efficiency; the efficiencies of PDR = 0.2 and PDR = 0.8 were almost the same. Therefore, only the simulation results with a PDR of 0.5–0.8 were analyzed in the present paper.

Different PDR values were closely related to the working mode and the size of gear ratio i_s and i_r of the DICPS. A high PDR allowed a decrease in the sun gear ratio i_s and an increase in the ring gear ratio i_r, resulting in an increase in the EM_S demand torque and a decrease in the EM_R demand torque, and changing the working mode of the DICPS. Figure 6 shows the working mode curves under different PDRs. The DICPS worked entirely in mode M2S when PDR was 0.5. When PDR = 0.65, the maximum torque of EM_S could not drive the DMET independently; the DICPS mainly worked in modes DMC and M1S. When PDR = 0.8, the DICPS worked entirely in mode DMC. It should be noted that for mode DMC, both motors were active at the same time, which means that both motors had power losses. Therefore, the longer the tractor was in mode DMC, the greater the power loss generated, and the lower the overall efficiency.

As can be seen from Figure 8, when PDR was 0.8, the DICPS worked in mode DMC for the longest time, followed by PDR = 0.65. When PDR was equal to 0.5, it worked in mode DMC for the shortest time and had the highest efficiency, so overall efficiency first increased, and then decreased. However, the overall efficiency of SMPS under the plowing cycle was 77.9%. Even in the worst-case DICPS scenario (PDR = 0.8, k = 7.6), its efficiency was still higher than the SMPS.

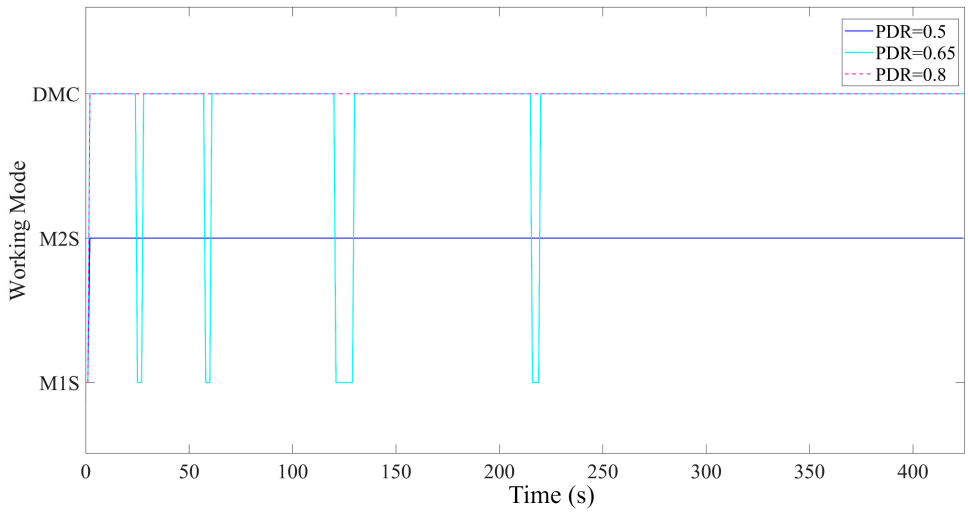

Figure 8. Working mode of the DICPS.

The motor speeds during the plowing cycle are shown in Figure 9. From the figure, it can be seen that the DICPS worked in the M2S mode at PDR = 0.5, which meant that the power demand of DMET could be met with the independent drive of EM_R while maintaining the highest overall efficiency. The DICPS worked in the DMC mode when PDR was 0.65 and 0.8, and, since the increase in PDR causes i_r to increase and i_s to decrease, the speeds of the two motors at PDR = 0.8 were greater than those at PDR = 0.65. The speed of the EM_T in the SMPS was lower than the EM_R in DICPS, because the total gear ratio of the SMPS was lower than that of the ring branch in the DICPS.

Figures 10–12 provide the operating points of the motors under the plowing cycle with different PDR values. To compare the influence of the same motor at different locations (sun gear or ring gear) on the economic performance of DICPS, the motors working points are put in the same figure, such as EM_S at PDR = 0.65 and EM_R at PDR = 0.35.

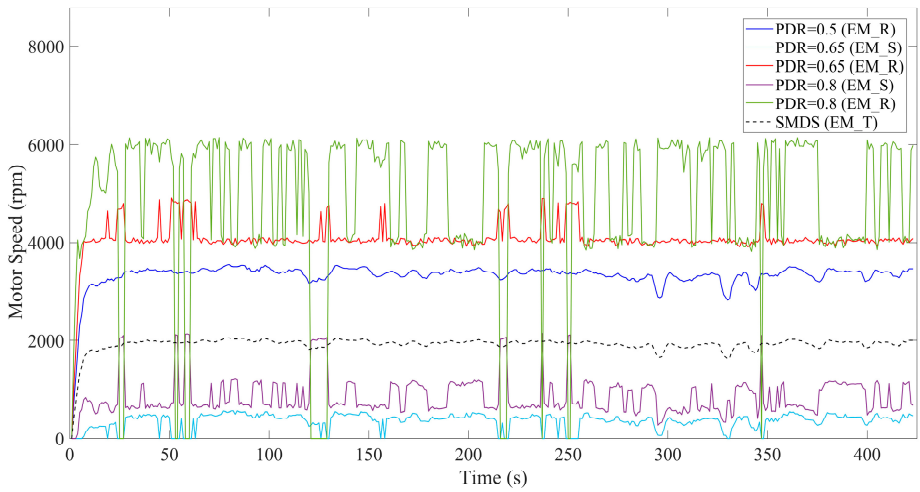

Figure 9. Speed of motors during the plowing cycle.

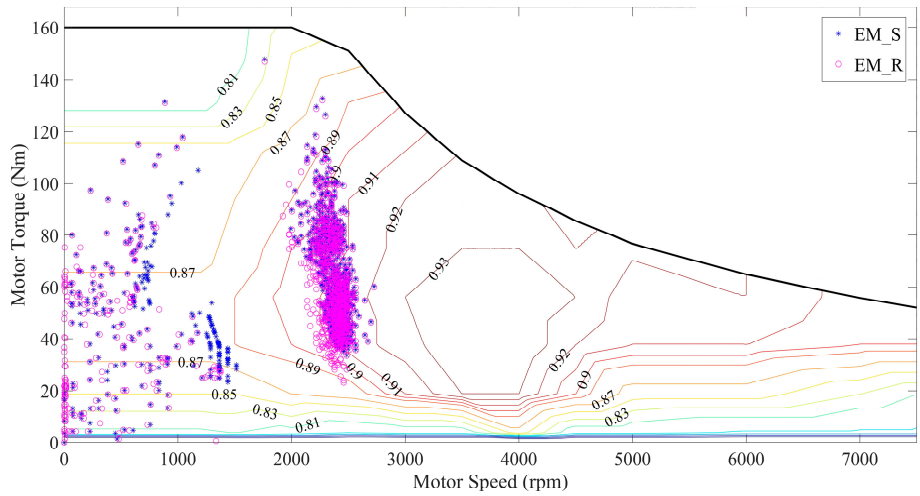

(**a**)

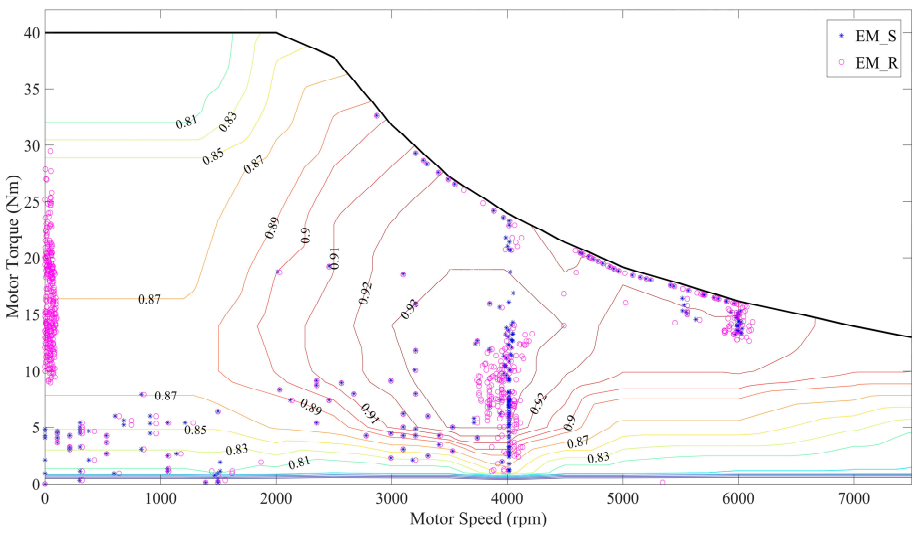

(**b**)

Figure 10. (**a**) Working points of EM_S at PDR = 0.8 and EM_R at PDR = 0.2; (**b**) working points of EM_S at PDR = 0.2 and EM_R at PDR = 0.8.

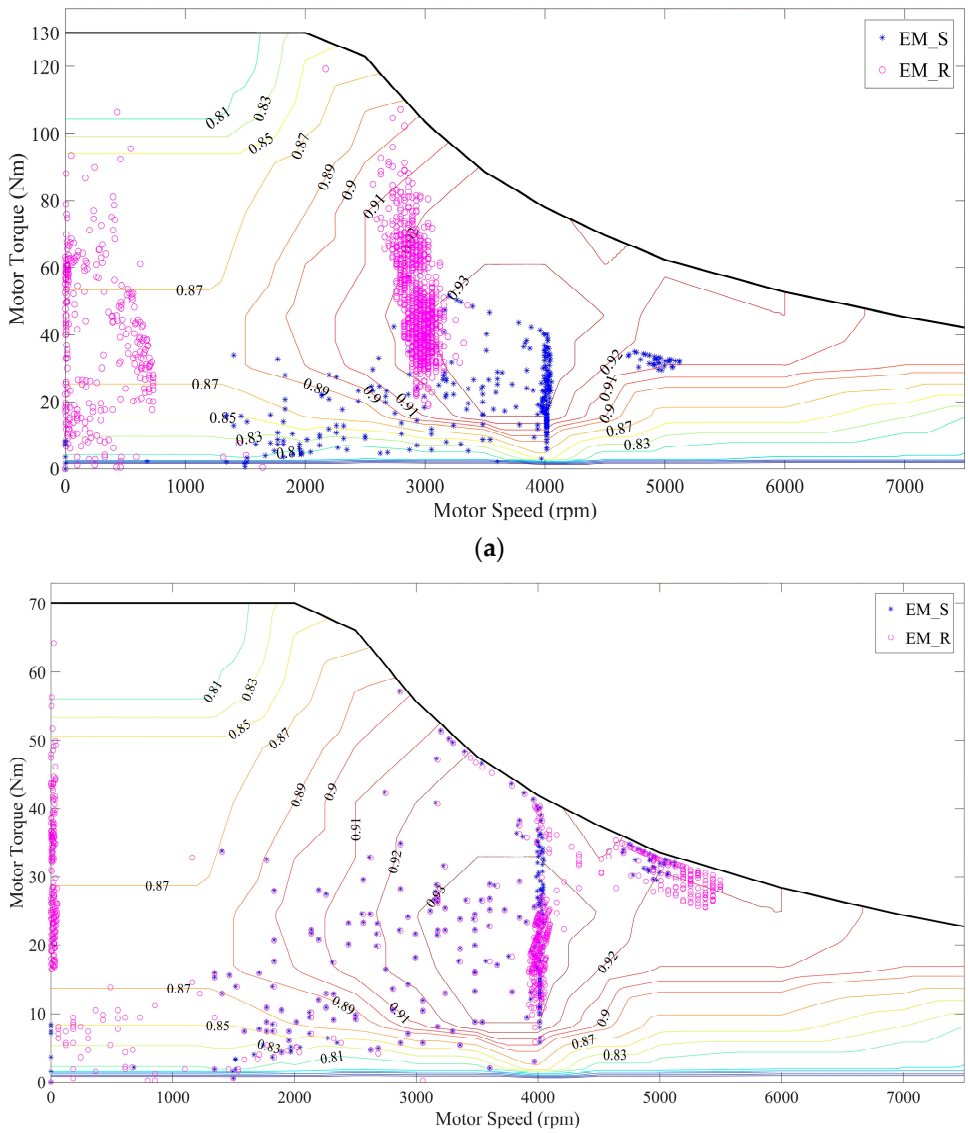

Figure 11. (**a**) Working points of EM_S at PDR = 0.65 and EM_R at PDR = 0.35; (**b**) working points of EM_S at PDR = 0.35 and EM_R at PDR = 0.65.

When the PDR was 0.8 or 0.2, the rated power of the motors in the DICPS was 24 kW and 6 kW, respectively. Figure 10a shows the working points of EM_S at PDR = 0.8 and EM_R at PDR = 0.2. The figure shows that the working points of EM_S and EM_R were distributed in a similar efficiency region, which means that they may have very close overall efficiencies. As can be seen from Figure 10b, EM_R at PDR = 0.8 had more working points distributed in the low-efficiency region than EM_S at PDR = 0.2. Therefore, PDR0.2 had a better economic performance than PDR0.8.

When PDR was equal to 0.65 or 0.35, the rated power of the motors in the DICPS was 19.5 kW and 10.5 kW, respectively. Figure 11a shows the working point distribution of EM_S at PDR = 0.65 and EM_R at PDR = 0.35. It can be seen that the change in the motor connection position resulted in a great change in the working points' distribution. When the motor was connected to the sun gear (i.e., EM_S at PDR = 0.65), the working points were located in the more efficient region, but the number of working points was much lower than that of EM_R. As seen in Figure 11b, many of the working points of EM_S and EM_R were distributed in a similar area, but the remaining working points of EM_R were mostly located in the low-efficiency region. Comparing Figures 10 and 11, it can be seen that

the working points in Figure 11, located in the high-efficiency region, were obviously greater than the motors in Figure 10. Therefore, when the PDR was equal to 0.35 or 0.65, the overall efficiency of the DICPS was higher than when the PDR was 0.2 or 0.8.

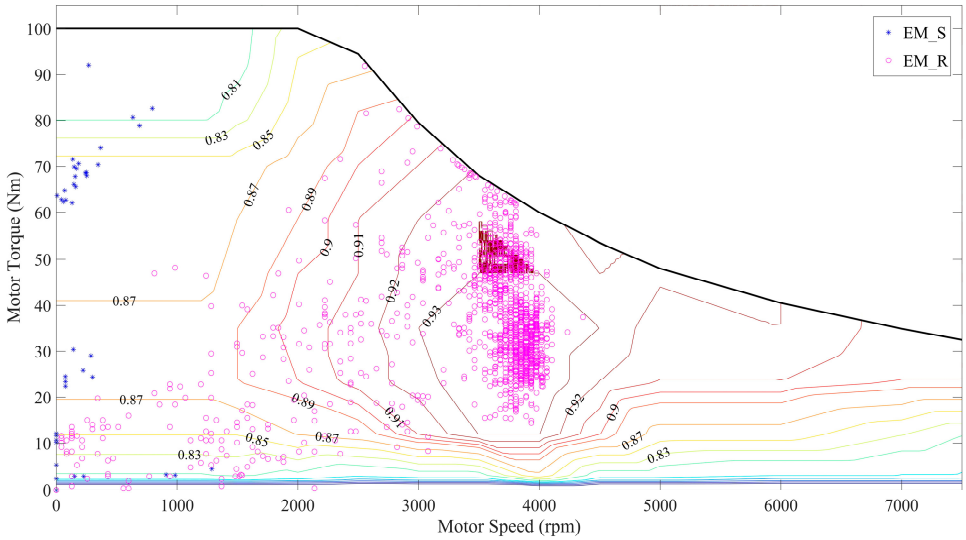

Figure 12. Working points of the motors at PDR = 0.5.

Figure 12 shows the working points of EM_S and EM_R at PDR = 0.5, and in this case the two motors were identical. There were few working points of EM_S, which indicates that the DICPS worked in mode M2S for most of the time. Most of the working points of EM_R were located in the high-efficiency region, which means that the DICPS had the highest efficiency at PDR = 0.5. In the case of PDR = 0.5, the parameter configuration with the highest overall efficiency was obtained through the calculation of EMS.

Figure 13 shows the working points of EM_T in the SMPS, and that the operating points were located in the low-speed region, which lowered the efficiency of the motor and thus reduced the overall efficiency. It can be seen that there were more working points for EM_S and EM_R in DICPS, with different PDRs located in the high-efficiency region compared to EM_T in the SMPS. Therefore, in the worst case, the overall efficiency of the SMPS was lower than that of the DICPS. The main reasons for the inefficiency of the SMPS are that when the tractor is plowing, the speed is basically constant and the gear position is almost unchanged, which means that the working points of EM_T are completely determined by the tractor load and cannot be adjusted. In addition, the use of mechanical gearboxes can also cause a lot of energy loss.

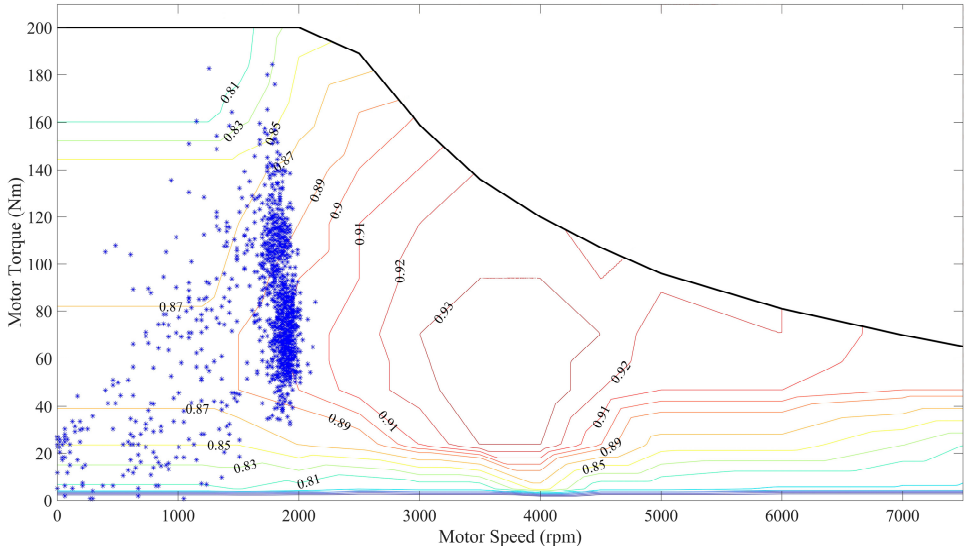

Figure 13. Working points of EM_T in SMPS.

The overall efficiency comparison under the plowing cycle is shown in Figure 14. It was noticeable that the overall efficiency values of the DICPS under three configurations are almost all greater than 85%. The overall efficiency was highest at PDR = 0.5, followed by 0.65, and PDR = 0.8 had the lowest efficiency. The SMPS had the lowest efficiency during the whole driving cycle, and the DICPS had about a 9.8% efficiency improvement compared to the SMPS.

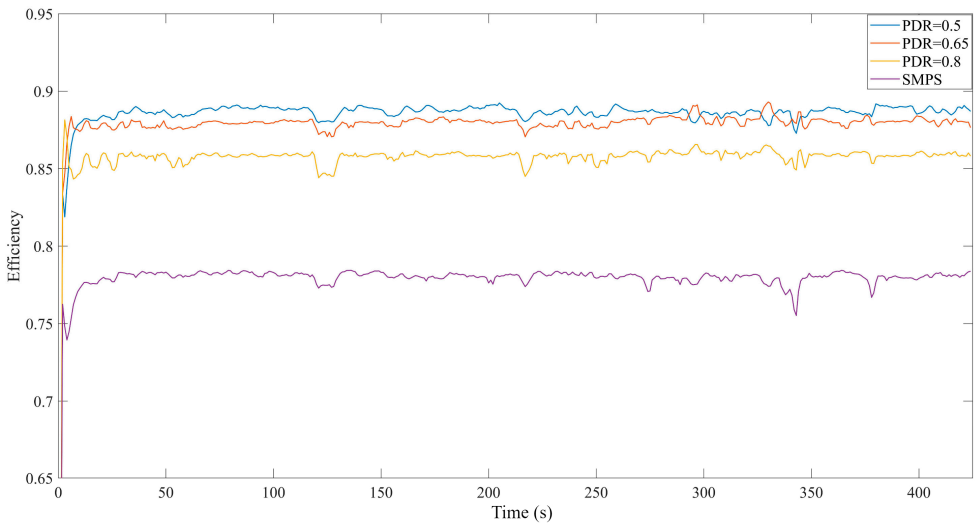

Figure 14. Overall efficiency comparison under plowing cycle.

3.2. Rotary Tillage Cycle

Rotary tillage is another common working condition of tractors with medium tractive work and heavy power demand. The traction resistance, tractor speed, and PTO power were measured in the previous field rotary tillage, as shown in Figure 15.

In rotary tillage operation, tractors overcome traction resistance to maintain their forward speed while providing stable output power for the power take-off (PTO), thus maintaining an approximately constant speed which requires two motors in a DICPS to drive independently, one of which provides the power required for DMET driving, and the other providing the power demand of the PTO. When rotary tillage is carried out, the PTO needs more power, so the PTO should be connected to the high-power motor. When PDR = 0.2–0.5, PTO is connected to EM_R, and when PDR = 0.5–0.8, PTO is connected

to EM_S. This section mainly studied the effects of different PDR and k values and PTO connection locations (connected to EM_S or EM_R) on the efficiency performance of the DICPS under a rotary tillage cycle.

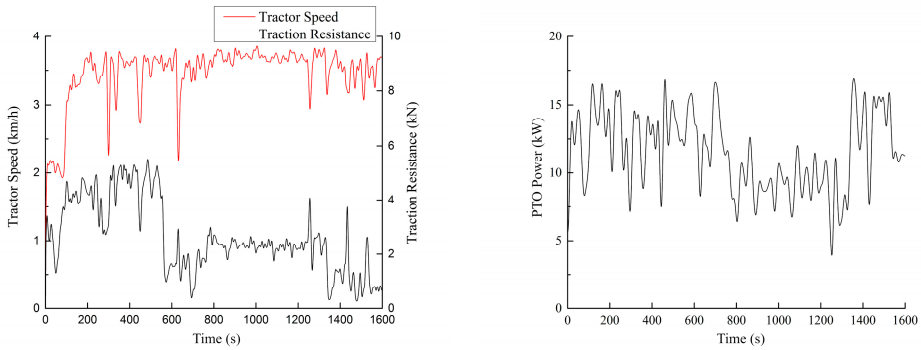

(**a**)Tractor speed and traction resistance (**b**) Demand power of PTO

Figure 15. Rotary tillage cycle for an agricultural tractor.

The overall efficiency at the end of the rotary tillage cycle for different PDR and k values is shown in Table 5. With the increase in k, the overall efficiency showed a decreasing trend, as it did under the ploughing cycle. As can be seen from Table 5, when the PTO was connected to EM_R, the overall efficiency decreased with the increase in PDR, and the overall efficiency had the same trend as PTO, connecting to EM_S. The maximum efficiency of the system occurred at PDR = 0.2.

Table 5. The overall efficiency of rotary tillage cycle.

	PDR = 0.2	PDR = 0.35	PDR = 0.5	PDR = 0.5	PDR = 0.65	PDR = 0.8
$k = 1.6$	86.1	84.2	82.8	85.8	85.2	84.3
$k = 3.6$	82.7	82	×	80.8	79.9	79.2
$k = 5.6$	81.8	80.9	×	×	×	×
$k = 7.6$	81.4	80.2	×	×	×	×

× indicates that the motors cannot meet the power demand.

The reason for this trend is that with the increase of PDR, i_s decreased and i_r increased (as shown in Table 3). A smaller i_s makes EM_S work in the low-speed and high-torque region, and a larger i_r makes EM_R work in the high-speed and low-torque region. Both motors deviate from the high-efficiency region. However, even for the worst-case (PDR = 0.8, $k = 3.6$) of the DICPS, the efficiency was still much higher than the best case of the SMPS.

When a tractor is working in rotary tillage, the power demand of the driving wheels is small and stable and the overall efficiency is mainly affected by the motor connected to the PTO. Therefore, this section mainly comprised a comparative study of the working points of the PTO motor with different PDR values. Figure 16a–c shows the working points of EM_S and EM_R with different PDR values under a rotary tillage cycle. Figure 16a shows the working point distribution of the motors when PDR was 0.8 or 0.2, and it can be seen that when PTO was connected to EM_R (PDR = 0.2), more working points were located in a higher efficiency region. When PTO was connected to EM_S, with the decrease in PDR, the working points of the motor shifted to the high-speed and low-torque area and gradually to the high-efficiency region; when PTO was connected to EM_R, with the increase in PDR, the working points of the motor were further away from the high-efficiency region, as shown in Figure 16b,c.

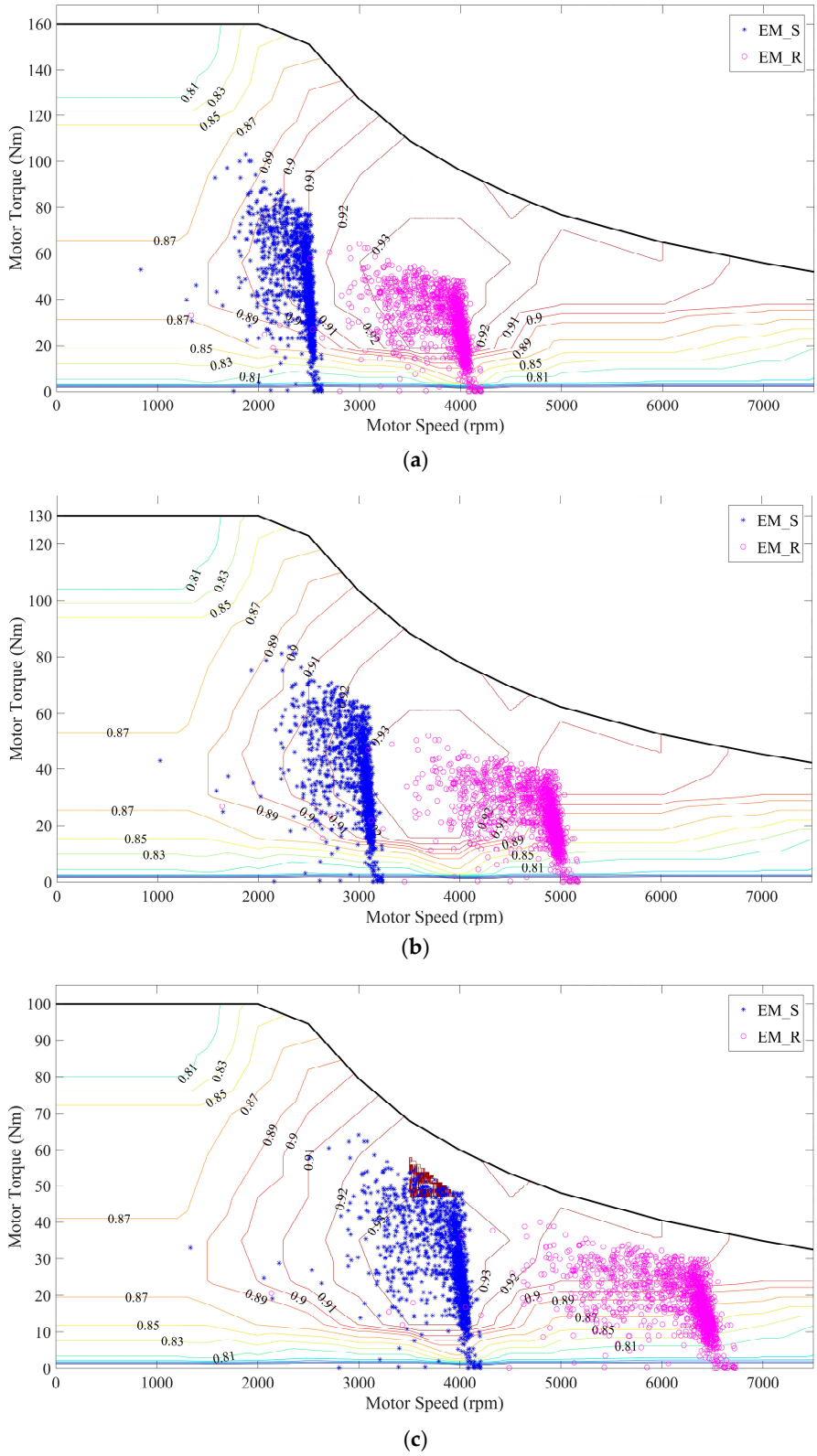

Figure 16. Working points of power take-off (PTO) motor with different PDR. (**a**) PDR = 0.8 or 0.2; (**b**) PDR = 0.65 or 0.35; (**c**) PDR = 0. 5.

The working point distribution of EM_T in the SMPS under the rotary tillage cycle is shown in Figure 17. It can be seen that more working points of EM_T were located in the low-efficiency region than in the motors in the DICPS, which resulted in the overall efficiency of the SMPS being lower than

that of the DICPS. The overall efficiency of SMPS under the whole cycle was 76.3%, which was 2.9% lower than the worst configuration of the DICPS.

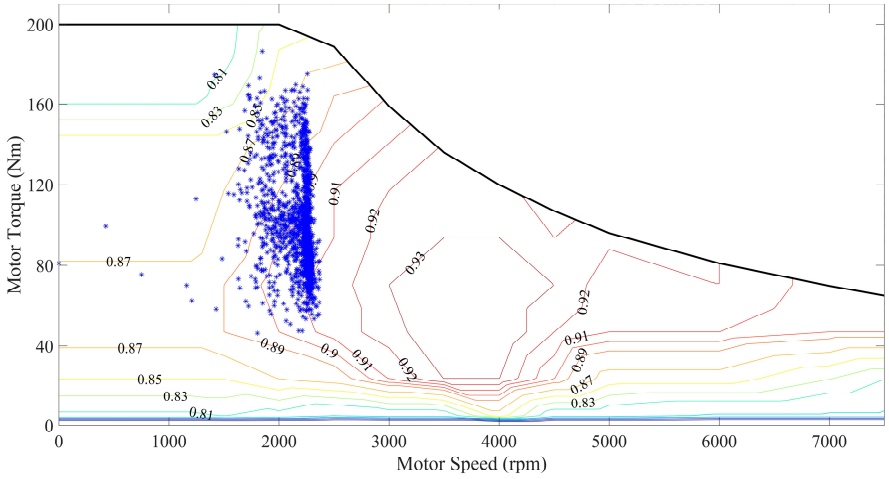

Figure 17. Working points of EM_T in the SMPS under rotary tillage cycle.

From the simulation of two typical working conditions, we found that different parameter configurations of DICPS led to changes in overall efficiency and the maximum difference in the overall efficiency was 6.6% (under rotary tillage cycle), which illustrated that the design and optimization of the powertrain parameters had a great impact on the economic performance of the DMET. According to the simulation results, the optimal parameters of DICPS were PDR = 0.5, k = 1.6, with the PTO shaft connected to the EM_S through the reduction gear. The DICPS had a much higher overall efficiency than the SMPS, demonstrating that dual-input coupling powertrains can effectively improve the energy efficiency of electric tractors.

4. Conclusions

In this study, a dual-input coupling powertrain system for PET was proposed to enhance economic performance. System models were constructed, including dynamic models and efficiency models. A matching design method was proposed to determine the feasible range of the structural parameters of the DICPS. To realize the efficient operation of the DICPS, an energy management strategy based on instantaneous efficiency optimization was formulated, including a power split strategy and a mode stability strategy. The simulation results showed that a high value of k will increase energy loss and decrease the overall efficiency under a plowing cycle and, with the increase in PDR, the energy loss will first decrease and then increase. When PTO is connected to EM_R or EM_S under a rotary tillage cycle, a high PDR can increase energy loss and decrease the overall efficiency. The trend of overall efficiency with parameter k was the same as the plowing cycle. It was also seen that the maximum difference of the overall efficiency under different parameter configurations was 6.6%, and the optimal parameters for the DICPS were configured as PDR = 0.5 and k = 1.6. Compared with the SMPS, the DICPS, with an optimal parameter configuration, improved overall efficiency by about 9.8%. In summary, this study can be used as a design reference theory for the powertrain system of DMET. Verification through practical experiments is part of our ongoing work.

Author Contributions: Conceptualization, B.X.; methodology, T.L., Z.L.; software, T.L.; validation, T.L. and J.L.; formal analysis, T.L.; investigation, J.L.; data curation, T.L.; writing—original draft preparation, T.L.; writing—review and editing, T.L. and Z.L.; supervision, B.X.; project administration, B.X. All authors have read and agreed to the published version of the manuscript.

Funding: This research was supported by the National Key Research and Development Plan of China (2016YFD0701001).

Conflicts of Interest: The authors declare no conflict of interest.

Nomenclature

Parameter	Explanation	Parameter	Explanation
m	tractor mass	I_s	equivalent inertia of the sun gear
g	gravity acceleration	I_c	equivalent inertia of the carrier
f	rolling friction coefficient	I_p	equivalent inertia of pinion relative to the center of mass
β	the angle between traction resistance and the horizontal direction	I_{ps}	equivalent inertia relative to the center of sun gear
r_q	road wheel radius	I_{m1}	equivalent inertia of EM_S
η_t	transmission efficiency	I_{m2}	equivalent inertia of EM_R
θ	incline angle of the road	T_{m1}	output torque of EM_S
F_T	traction resistance	T_{m2}	output torque of EM_R
F_{total}	total resistance on the tractor	$T_{\max 1}$	maximum output torque of EM_S
λ	penalty factor	$T_{\max 2}$	maximum output torque of EM_R
v_a	actual velocity	T_L	driving resistance torque
i_s	reduction gear of sun gear motor	T_c	output torque of the carrier
i_r	reduction gear of ring gear motor	T_r	output torque of the ring gear
i_m	main reduction gear	T_s	output torque of the sun gear
i_f	final reduction gear	ω_{m1}	rotational speed of EM_S
k	characteristic parameter of planetary gear set	ω_{m2}	rotational speed of EM_R
Z	number of plowshares	$\omega_{\max 1}$	maximum rotational speed of EM_S
b_1	width of ploughshare	$\omega_{\max 2}$	maximum rotational speed of EM_S
h_s	tillage depth	ω_c	rotational speed of carrier
s_r	soil-specific resistance	P_e	instantaneous energy consumption of battery
I_r	equivalent inertia of the ring gear	$P_{\max 1}$	maximum output power of EM_S
U_{oc}	battery open circuit voltage	$P_{\max 2}$	maximum output power of EM_R
R_{bat}	internal resistance	$P_{e_current}$	instantaneous energy consumption of battery in the current working mode
Q_{bat}	capacity of battery	P_{e_other}	instantaneous energy consumption of battery in the non-working modes
P_{bat}	output power of the battery	η_o	overall efficiency

Abbreviations

DICPS	Dual-input coupling powertrain system
PET	Pure electric tractors
EMS	Energy management strategy
DMET	Dual-motor driven electric tractor
SMPS	Single-motor powertrain system
PMP	Pontryagin's minimum principle
DP	Dynamic programming
PTO	Power take-off
M1S	EM_S independent drive
M2S	EM_R independent drive
DMC	Dual-motor coupling drive

References

1. Xie, B.; Wu, Z.; Mao, E. Development and prospect of key technologies on agricultural tractor. *Trans. CSAM* **2018**, *49*, 1–17. [CrossRef]
2. Lee, D.; Kim, Y.; Choi, C.; Chung, S.; Inoue, E.; Okayasu, T. Development of a Parallel Hybrid System for Agricultural Tractors. *J. Fac. Agric. Kyushu Univ.* **2017**, *62*, 137–144.

3. Moreda, G.P.; Munoz-Garcia, M.A.; Barreiro, P. High voltage electrification and agricultural machinery—A review. *Energy Convers. Manag.* **2016**, *115*, 117–131. [CrossRef]
4. Magalhães, R.O.; Assunção, M.V.; Santos, J.P.; Silva, E.V.; Ferreira, L.G.; Magalhães, R.R.; Ferreira, D.D. Review on applications of electric vehicles in the countryside. *Ciênc. Rural* **2017**, *47*. [CrossRef]
5. Ueka, Y.; Yamashita, J.; Sato, K.; Doi, Y. Study on the development of the electric tractor specifications and traveling and tilling performance of a prototype electric tractor. *EAFF* **2013**, *6*, 160–164. [CrossRef]
6. Volpato, C.E.S.; Paula, V.R.; Barbosa, J.A.; Volpato, E.L. Evaluation of the Operational Viability of the Use of Electricity as a Source of Power in Agricultural Tractors. *ASABE Ann. Int. Meet.* **2016**. [CrossRef]
7. Chen, L.; Zhan, Q.; Wang, W.; Huang, X.; Zheng, Q. Design and Experiment of Electric Drive System for Pure Electric Tractor. *Trans. CSAM* **2018**, *49*, 388–393. [CrossRef]
8. Molari, G.; Sedoni, E. Experimental evaluation of power losses in a power-shift agricultural tractor transmission. *Biosyst. Eng.* **2008**, *100*, 177–183. [CrossRef]
9. Zhang, S.; Xiong, R.; Zhang, C. Pontryagin's Minimum Principle-based power management of a dual-motor-driven electric bus. *Appl. Energy* **2015**, *159*, 370–380. [CrossRef]
10. Zhang, C.; Zhang, S.; Han, G.; Liu, H. Power Management Comparison for a Dual-Motor-Propulsion System Used in a Battery Electric Bus. *IEEE Trans. Ind. Electron.* **2017**, *64*, 3873–3882. [CrossRef]
11. Hu, J.; Zu, G.; Jia, M.; Niu, X. Parameter matching and optimal energy management for a novel dual-motor multi-modes powertrain system. *MSSP* **2019**, *116*, 113–128. [CrossRef]
12. Tseng, S.; Tseng, C.; Liu, T.; Chen, J. Wide-range adjustable speed control method for dual-motor drive systems. *IET Electr. Power Appl.* **2015**, *9*, 107–116. [CrossRef]
13. Lee, H.; Kim, J.; Park, Y.; Cha, S. Rule-Based Power Distribution in the Power Train of a Parallel Hybrid Tractor for Fuel Savings. *Int. J. Precis. Eng. Manuf.* **2016**, *3*, 231–237. [CrossRef]
14. Deng, X.; Zhu, S.; Gao, H.; Zhang, Y. Design Theory and Method for Drive Train of Hybrid Electric Tractor. *Trans. CSAM* **2012**, *43*, 24–31. [CrossRef]
15. Xu, L.; Liu, M.; Zhou, Z. Design of drive system for series hybrid electric tractor. *Trans. CSAE* **2014**, *30*, 11–18. [CrossRef]
16. Gao, H. Researches on Drive System of Electric Tractor. Ph.D. Thesis, Nanjing Agricultural University, Nanjing, China, 2008.
17. Chen, Y.; Xie, B.; Du, Y.; Mao, E. Powertrain parameter matching and optimal design of dual-motor driven electric tractor. *Int. J. Agric. Biol. Eng.* **2019**, *12*, 33–39. [CrossRef]
18. Wu, J.; Liang, J.; Ruan, J.; Zhang, N.; Walker, P. A robust energy management strategy for EVs with dual input power-split transmission. *MSSP* **2018**, *111*, 442–455. [CrossRef]
19. Zhang, S.; Xiong, R.; Zhang, C.; Sun, F. An optimal structure selection and parameter design approach for a dual-motor-driven system used in an electric bus. *Energy* **2016**, *96*, 437–447. [CrossRef]
20. Jia, C.; Qiao, W.; Qu, L. Numerical Methods for Optimal Control of Hybrid Electric Agricultural Tractors. *ITEC* **2019**, 1–6. [CrossRef]
21. Benford, H.; Leising, M. The Lever Analogy: A New Tool in Transmission Analysis. *SAE Trans.* **1981**, *90*, 429–437.
22. Pennestrì, E.; Mariti, L.; Valentini, P.; Mucino, V. Efficiency evaluation of gearboxes for parallel hybrid vehicles: Theory and applications. *Mech. Mach. Theory* **2012**, *49*, 157–176. [CrossRef]
23. Zhou, Y. *Theory of Automobile and Tractor*; China Agricultural University Press: Beijing, China, 2000.
24. Han, G. Integrated Control and Parameters Optimization of Dual-Motor Planetary Coupling Driving System for Electric Buses. Ph.D. Thesis, Beijing Institute of Technology, Beijing, China, 2015.
25. Verstraten, T.; Furnémont, R.; López-García, P.; Rodriguez-Cianca, D.; Cao, H.-L.; Vanderborght, B. Modeling and design of an energy-efficient dual-motor actuation unit with a planetary differential and holding brakes. *Mechatronics* **2018**, *49*, 134–148. [CrossRef]

© 2020 by the authors. Licensee MDPI, Basel, Switzerland. This article is an open access article distributed under the terms and conditions of the Creative Commons Attribution (CC BY) license (http://creativecommons.org/licenses/by/4.0/).